Analysis of delamination of non-homogeneous composite structures considering an interfacial decohesion model

M. Grafen, H. Rapp, Institut für Leichtbau, Universität der Bundeswehr München, Germany

Summary

This paper deals with the delamination of non-homogeneous composite structures. A bonded joint loaded in shear is considered. The adherends are described by the theory of an elastic bar. An exponential material model is used for analysing delamination failure in the adhesive layer. This model is also able to take decohesion into account. The stresses in the adhesive layer between two adherends are characterized by a traction displacement relation. The stiffness of these interface is defined by the energy release rate and a strength parameter σ_{max}. For simplification a linear approach of the decohesion model is made. The resulting system of first order linear differential equations is solved and leads to the transfer matrix method. Non-homogeneous transverse crack tension specimens are designed. Force displacement curves of the specimens are recorded and compared with numerical results.

1 Introduction

Composite structures are prone to delamination. In tapered laminates the stiffness of each layer has a great influence on the delamination strength. The most simple form of a tapered laminate is the lap joint (Figure 1).
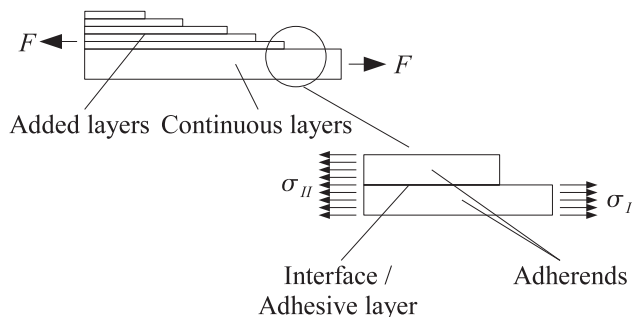

Figure 1: Tapered laminate (left) and lap joint (right)

Adhesive joints can be used as an efficient analogous model to compute delamination. In [5] the stresses in a bonded joint are described by using the theory of plane strain. It is assumed that the elastic behaviour of a thin adhesive layer has a marginal influence on the stresses in the adherends.

An orthotropic material can also be used to describe the stresses in the adhesive layer [2], [3]. This approach leads to differential equations, which have to be solved. For this stress analysis, specific data like thickness, strength and stiffness of the adhesive layer are needed. It is very difficult to determine these unknown properties for laminates.

Instead it is possible to use methods of linear elastic fracture mechanics (LEFM). The unknown specific properties can be replaced by the energy release rate (ERR) in order to compute delamination [11]. So the advantage of LEFM is that only one instead of three parameters is needed. Additionally it is very easy to determine the energy release rate with fracture tests. Consequently, for strength analysis of bonded joints with LEFM the adhesive layer has to be described by material models which are able to take fracture mechanics into account [1], [7]. These decohesion models are based on LEFM in that way that the separation work for interfacial decohesion is equal to the ERR. In order to describe the restoring traction in the interface an additional strength parameter σmax is used. The use of σmax as a second parameter is different from pure LEFM. As a consequence the decohesion model seems to be impractical. In opposite to pure fracture mechanics or stress analysis, decohesion models are able to differentiate between damage and fracture. A damage or decohesion is distinguished by a softening of the stiffness of the interface. The fracture or crack is characterized by stiffness zero. The two adherends are no more bonded to each other.

Decohesion models are already used in finite element analysis (e.g. [1], [4]). These analysis are often two- or threedimensional. For this reason, the number of degrees of freedom (DOF) and the computing time are very high. The use of a one-dimensional approach reduces the DOF. So the theory of an elastic bar is useful to describe the deformation of the adherends.

2 Analytical solution

In order to get an analytical solution material law and equilibrium equation have to be used.

2.1 Equilibrium equation

A bonded joint of two adherends is considered. The adherends have the Young's modulus E_1 and E_2, the thickness t_1 and t_2 (Figure 2). The width runs in y-direction. The joint is loaded by axial membrane forces N_x (force per width). It is assumed that the adhesive layer has

to transfer shear stresses τ only. The thickness of the adhesive layer is neglected, because it is small compared to the thickness of the adherends. The analysis of the equilibrium leads to
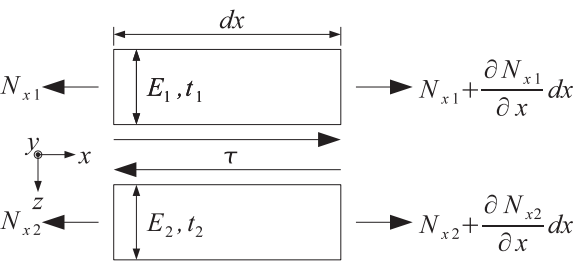
$$(1) \qquad \frac{\partial N_{x1}}{\partial x} = -\frac{\partial N_{x2}}{\partial x} = -\tau .$$

Figure 2: Bonded joint under normal load

The elastic behaviour of the adherends is given by

$$(2) \qquad N_x = EA\,u'$$

where u denotes the deformation in x-direction, E is the Young's modulus and A the cross section area [6]. The prime describes the differentiation $d(\,)/dx$.

2.2 Decohesion model

If specific values like thickness or stiffness of an adhesive layer are not known, it is useful to describe the deformation of the adhesive layer by a displacement jump δ over the interface (Figure 3).

The points P_1 and P_2 in an unloaded bonded joint can be assumed as coincident, if the thickness of the adhesive layer is small compared to the thickness of the adherends. If the joint is loaded by axial forces, these points are moving from P_1 and P_2 to $\overline{P}_1$ and $\overline{P}_2$.

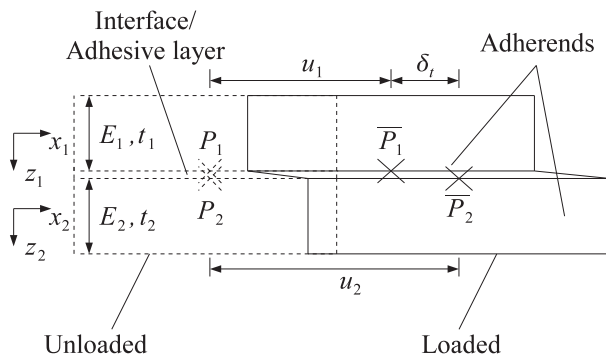Figure 3: Displacement jump in a bonded joint

The difference of the two displacements u_1 and u_2 of the adherends is equal to δ_t:

$$(3) \qquad \delta_t = u_2 - u_1 .$$

Because of pure shear load in the bonded joint, the normal displacement jump δ_n is assumed to be zero.

An exponential model for the elastic material behaviour, which is presented in [7], can be used to describe stresses in an interface by using a potential Φ

$$(4) \quad \Phi(\delta_n,\delta_t) = \sigma_{max} e \overline{\delta}_n \left(1 - \left[1 + \frac{\delta_n}{\overline{\delta}_n} \right] e^{-\frac{\delta_n}{\overline{\delta}_n}} e^{-\left(\frac{\delta_t}{\overline{\delta}_t}\right)^2} \right)$$

as a function of the displacement jumps δ_n and δ_t.

The shear stresses τ are computed by differentiating Φ with respect to δ_t:

$$(5) \qquad \tau = \frac{\partial \Phi}{\partial \delta_t}(\delta_n = 0) = 2\sigma_{max} e \frac{\overline{\delta}_n}{\overline{\delta}_t} \frac{\delta_t}{\overline{\delta}_t} e^{-\left(\frac{\delta_t}{\overline{\delta}_t}\right)^2} .$$

In (4) and (5) σ_{max} denotes a strength parameter with the dimension N/mm^2 and e the Euler's number. The term $\overline{\delta}_t$ describes the location of the maximum of τ. The parameter $\overline{\delta}_t$ can be computed by

$$(6) \qquad \frac{\partial \tau}{\partial \delta_t} = 0 ,$$

which leads to

$$(7) \qquad \delta_t = \frac{\sqrt{2}}{2} \overline{\delta}_t .$$

The maximum shear stress τ is given by

$$(8) \qquad \tau(\delta_t = \frac{\sqrt{2}}{2} \overline{\delta}_t) = \sigma_{max} e \frac{\overline{\delta}_n}{\overline{\delta}_t} \sqrt{\frac{2}{e}} .$$

Figure 4 shows the normalized shear stress τ/τ_{max} versus the displacement jump δ_t.
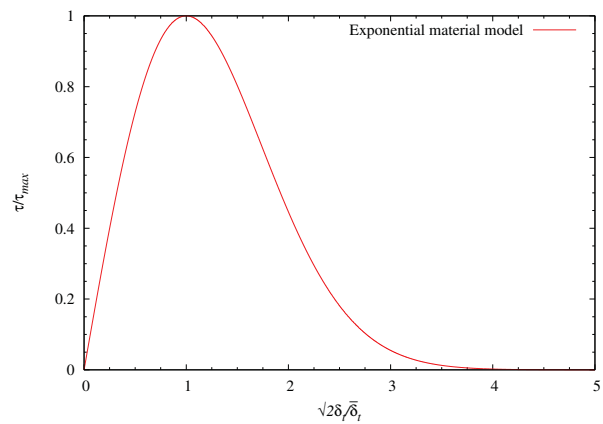

Figure 4: Exponential material model

The separation work, which is assumed to be equal to the energy release rate G_c, is computed as

$$(9) \quad G_C = \int_0^\infty \tau d\delta_t = \sigma_{max} e \bar{\delta}_n = \tau_{max} \sqrt{\frac{e}{2}} \bar{\delta}_t .$$

So it is observable that $\bar{\delta}_t$ follows from the energy release rate G_c.

Normalizing the shear stress τ with respect to τ_{max} (Equation (8) and (9)) has the advantage that the parameter δ_n for a normal separation is cancelled when doing a pure shear stress analysis. Though $\bar{\delta}_t$ has the dimension of length it does not necessarily have to be a proportion of the analysed bonded joint.

For simplification it is useful to make a bi-linear approach $\tau(\delta_t) = m\delta_t + c$ of (5). The slope m and a constant value c can be computed by two assumptions:

- The bi-linear approach and the exponential model (5) should have the points $\tau(\delta_t = 0) = 0$ and $\tau(\delta_t = \sqrt{2}/2\, \delta_t) = \tau_{max}$ in common.

- The area under the function $\tau(\delta_t)$ is equal to the energy release rate.

These two assumptions lead to the bi-linear equation

$$(10)$$

$$\tau = \begin{cases} \dfrac{\tau_{max}}{\bar{\delta}_t}\delta_t & 0 < \delta_t < \bar{\delta}_t \\[2mm] -\dfrac{\tau_{max}}{\delta_{t\,max} - \bar{\delta}_t}\delta_t + \dfrac{\tau_{max}}{\delta_{t\,max} - \bar{\delta}_t}\delta_{t\,max} & \bar{\delta}_t < \delta_t < \delta_{t\,max} \\[2mm] 0 & \delta_{t\,max} < \delta_t \end{cases}$$

and

$$(11) \quad G_C = \frac{1}{2}\tau_{max}\delta_{t\,max} .$$

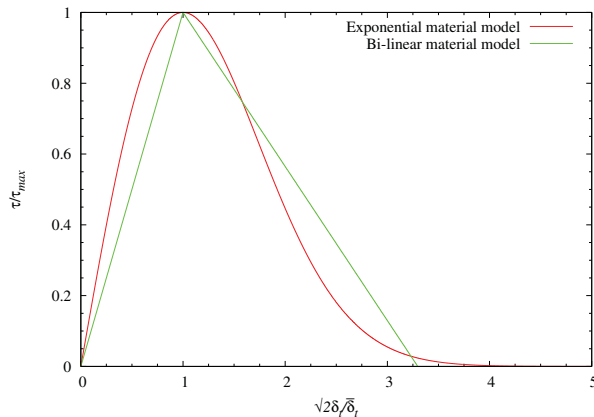A comparison of the bi-linear and the exponential model is shown in Figure 5.

Figure 5: Exponential and bi-linear material model

The line from $0 < \delta < \bar{\delta}_t$ describes an intact interface between the two adherends. $\bar{\delta}_t < \delta < \delta_{max}$ the line denotes decohesion or damage and for $\delta_{max} < \delta$ fracture or crack. Bi-linear models are already presented in [4] to analyse the delamination of composites in finite element analysis. A linear system of differential equations can be developed by using (2), (3) and (10):

$$(12)$$

$$\begin{Bmatrix} u_1 \\ N_{1x} \\ u_2 \\ N_{2x} \end{Bmatrix}' = \begin{bmatrix} 0 & \frac{1}{E_1 A_1} & 0 & 0 \\ K_t & 0 & -K_t & 0 \\ 0 & 0 & \frac{1}{E_1 A_2} & 0 \\ -K_t & 0 & K_t & 0 \end{bmatrix} \begin{Bmatrix} u_1 \\ N_{1x} \\ u_2 \\ N_{2x} \end{Bmatrix} + \begin{Bmatrix} 0 \\ -l_t \\ 0 \\ l_t \end{Bmatrix} .$$

The values of K_t and l_t for the different regions of the bi-linear model are given in Tab 1. Abbreviated, the linear differential equation system (12) can be written as

$$(13) \quad z'(x) = Kz(x) + l(x) .$$

	K_t	l_t
$0 < \delta_t < \bar{\delta}_t$	$\dfrac{\tau_{max}}{\bar{\delta}_t}$	0
$\bar{\delta}_t < \delta_t < \delta_{t\,max}$	$-\dfrac{\tau_{max}}{\delta_{t\,max} - \bar{\delta}_t}$	$\dfrac{\tau_{max}}{\delta_{t\,max} - \bar{\delta}_t}\delta_{t\,max}$
$\delta_{t\,max} < \delta_t$	0	0

Tab 1: Values of K_t and l_t

2.3 Transfer Matrix Method

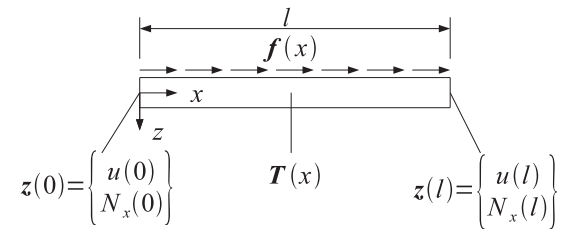The main principal of the transfer matrix method is shown in Figure 6.

Figure 6: Bar with state variables

If the state vector $z(0)$ at the position 0, the transfer matrix $T(x)$ and the load vector $f(x)$ is known, the state at position l can be computed by

$$(14) \quad z(l) = T(x)z(0) + f(x) .$$

In order to apply the transfer matrix method to solve the delamination problem (12) the transfer matrix $T(x)$ and the load vector $f(x)$ have to be determined. For a linear differential equation system as it is given in (12), a solution is

$$(15) \qquad z(x) = e^{Kz(x)} + e^{Kz(x)} \int_0^x e^{-Kz(\xi)} l(\xi) d\xi .$$

The comparison of (14) and (15) shows

$$(16) \qquad T(x) = e^{Kx}$$

and

$$(17) \qquad f(x) = e^{Kx} \int_{\xi=0}^{\xi=x} e^{-K\xi} l(\xi) d\xi .$$

The transfer matrix $T(x)$ can be calculated by the series expansion of e^x with

$$(18) \qquad T(x) = e^{Kx} = \sum_{i=0}^{\infty} \frac{1}{i!} K^i x^i$$

or by the theorem of Caley-Hamilton [8]. It has to be noted that (15) is an analytical solution to (12), even if the transfer matrix is calculated numerically.

For the numerical analysis of the delamination process several transfer sections have to be used (Figure 7).
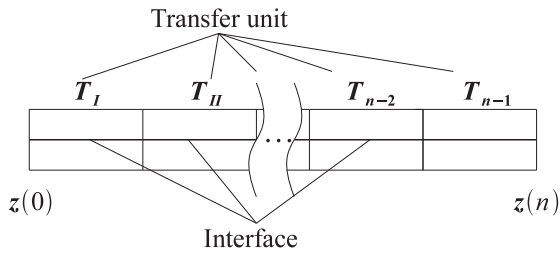

Figure 7: Transfer-Model for a bonded joint

This is founded in the fact that over the whole analysed structure are areas with decohesion and fracture. The analytical solution (12) is only able to describe one of these conditions depending on the values K_t and l_t from Tab 1.

In order to avoid numerical problems (14) is converted to

$$(21) \qquad T_n z_n - I z_{n+1} = -f_n .$$

This allows to calculate all unknown state parameters z_n in a single system of linear equations by setting the boundery conditions (BC):

(22)

$$\begin{bmatrix} T_1 & -I & 0 & 0 & \cdots & 0 & 0 \\ 0 & T_2 & -I & 0 & \cdots & 0 & 0 \\ 0 & 0 & T_3 & -I & \cdots & 0 & 0 \\ \vdots & \vdots & \vdots & \vdots & \ddots & \vdots & \vdots \\ 0 & 0 & 0 & 0 & \cdots & T_n & -I \\ BC & BC & BC & BC & BC & BC & BC \end{bmatrix} \begin{Bmatrix} z_1 \\ z_2 \\ z_3 \\ \vdots \\ z_n \\ z_{n+1} \end{Bmatrix} = \begin{Bmatrix} -f_1 \\ -f_2 \\ -f_3 \\ \vdots \\ -f_n \\ BC \end{Bmatrix} .$$

The system of equations is solved for each displacement increment beginning with $u = 0$ mm until u_{max} by using Gaussian elimination. For each transfer section T_i the displacement-jump δ_t is analysed and K_t and l_t is set according to Tab 1. A new displacement increment is added and the resulting system of equations is solved.

The result of an analysis with $G_C = 1.5$ N/m, $E_1 t_1 = E_2 t_2 = 24000$ Nmm, $\tau_{max} = 80$ N/mm^2, $l = 50$ mm, width 25 mm, 500 increments and the number of transfer units $n = 90$ is shown in Figure 8.
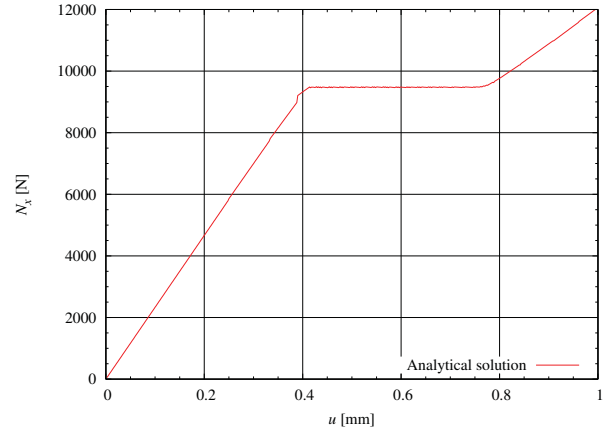

Figure 8: Solution of transfer matrix method

A linear slope from $u = 0$ mm to $u = 0.4$ mm and a plateau at a level of $N_x = 9500$ N is observable. At a displacement of $u = 0.75$ mm a second linear slope can be seen. The meanings of the several areas are explained in the comparison with experimental results in 3.2. A small non-linearity is observable at $u = 0.4$ mm, which is caused by numerical problems.

3 Experimental Results

The analytical solution (12) has to be verified by experimental results. For pure shear load in laminates Transverse crack tension (TCT) specimens are suitable (Figure 9).
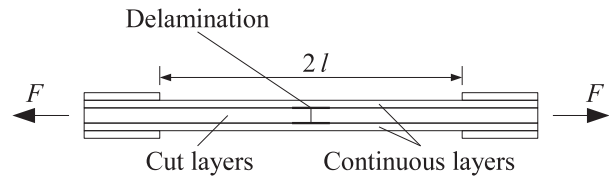

Figure 9: Transverse crack tension specimen

3.1 Design of specimen

The specimen is designed for delamination failure. The continuous layers made of glass fibre reinforced plastic (GFRP) and the cut layers are made of carbon fibre reinforced plastic (CFRP). Loaded in tension this leads to shear stresses between the cut and the continuous layers. If the shear stress is too high, delamination will occur.

According to [11] or [13], for a bonded lap joint with an adhesive layer (Figure 10), the energy release rate can be computed from

$$(23) \qquad \varepsilon_I = \sqrt{2G_c \frac{E_1 t_1 + E_2 t_2}{E_1 t_1 E_2 t_2}} \ .$$
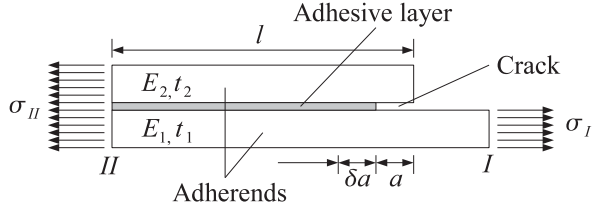

Figure 10: Bonded lap joint

With (2) and the correlation between the strain at the location *I* and *II*

$$(24) \qquad \varepsilon_I = \varepsilon_{II} \frac{E_1 t_1 + E_2 t_2}{E_2 t_2} \ .$$

the displacement u_c at *II* at the beginning of the delamination can be calculated to

$$(25) \qquad u_c = \varepsilon_{II} l = l \sqrt{2G_c \frac{E_2 t_2}{E_1 t_1 (E_1 t_1 + E_2 t_2)}} \ .$$

With the equilibrium $\sigma = N_x/A$ the force is computed as

$$(26) \qquad N_x = \varepsilon_I E_1 A_1 = E_1 A_1 \sqrt{2G_c \frac{E_1 t_1 + E_2 t_2}{E_1 t_1 E_2 t_2}} \ .$$

In order to avoid fibre-failure of the continuous layers, the minimum strain of (23) is searched. This exists for

$$(27) \qquad E_1 t_1 = E_2 t_2 \ .$$

The parameter *k* denotes the number of plies and t_p denotes the thickness of each ply. If the number of the continuous layers k_2 is set, k_1 is given as

$$(28) \qquad k_1 = \frac{E_2 t_{p2} k_2}{E_1 t_{p1}} \ .$$

For the computation of the number of plies laminate theory [12] and the material properties in Tab 2 are used.

Fabric	Fibre weight per area	Fibre density	Fibres Young's modulus
Glass Fibre	$0.280 \frac{kg}{m^2}$	$2.6 \frac{g}{cm^3}$	$73000 \frac{N}{mm^2}$
Carbon Fibre	$0.204 \frac{kg}{m^2}$	$1.78 \frac{g}{cm^3}$	$230000 \frac{N}{mm^2}$

Tab 2: Fibre material properties [10], [9]

The fibre volume content φ_f is accepted to be 0.45. Setting the layer number $k_1 = 3$, equation (28) provides $k_2 = 9$. Using a 0°/90° ply set-up, laminate theory gives $E_1 = 21200$ N/mm^2, $t_{p1} = 0.255$ mm, $E_2 = 56000$ N/mm^2, $t_{p2} = 0.240$ mm. With these parameters and $G_c = 1.5$ N/m, σ_{II} is 247.30 N/mm^2. This is less than an accepted fibre-failure at 800 N/mm^2 in the glass fibre layer [14].

The specimens were made by using the vacuum bag technology [10]. At a first step, a 250 mm x 200 mm plate for the cut layers is laminated by hand. After curing, these layers are cut in two pieces and put between the continuous layers. As a next step about 25 mm wide specimens are made, whose cut edges are flattened to reduce stress peeks. After fabrication, a thickness $t_1 = 0.75$mm, $t_2 = 1.95$ mm and a width of 23.4 mm and a length of $l = 65$ mm is measured. This leads to the fibre volume-content $\varphi_{f1} = 0.497$, $\varphi_{f2} = 0.458$ and a Young's modulus $E_1 = 23410$ N/mm^2 and $E_2 = 57056$ N/mm^2 respectively.

3.2 Tests

The tests are made on Z150 testing machine from "Zwick Roell" and run with a cross head speed of 2 mm/min. A test set-up is shown in Figure 11.
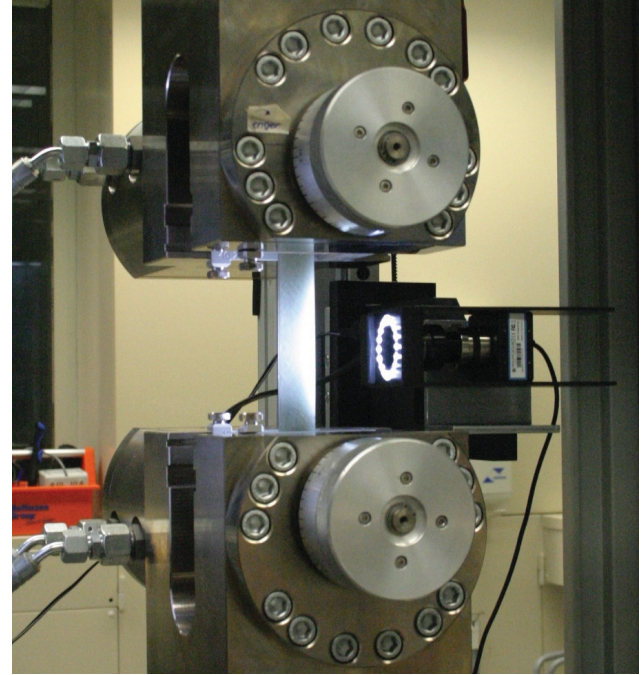

Figure 11: Test set-up

Displacements and forces are recorded. A video for visual analysis of the delamination process is recorded too. Selected results are shown in Figure 12, 13 and 14.
A Young's modulus about 31000 N/mm^2 is measured by a Digital Clip-On Extensometer. This value is close to the mixed Young's modulus

$$(29) \qquad E_{mix} = \frac{E_1 t_1 + E_2 t_2}{t_1 + t_2} = 32756 \, \frac{\text{N}}{\text{mm}^2}$$

of both adherends. With the assumption that the deformation of the testing machine is proportional to the measured cross head displacement, the value E_{mix} is used to separate the deformation of the testing machine from the measured displacement.

An almost linear slope between $u = 0$ mm to $u = 0.75$ mm is observable. This is due to an intact interface between the cut and the continuous layers as shown in Figure 13. Both layers are loaded by axial force.
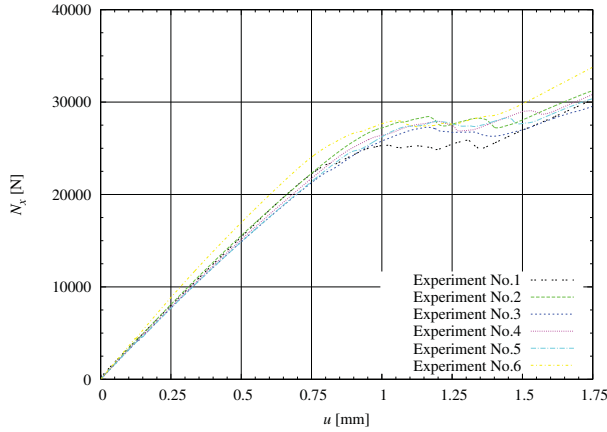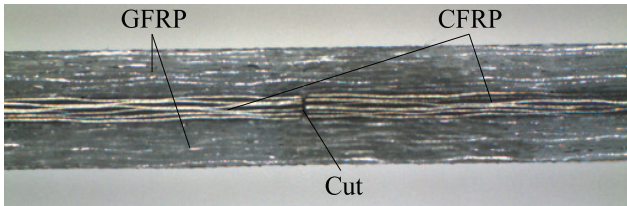

Figure 12: Experimental results

Figure 13: Picture of specimen 2 at 11506 N

A constant load plateau at about $N_x = 27500$ N is also observable. This is the result of a delamination process between the two adherends as shown in Figure 14.
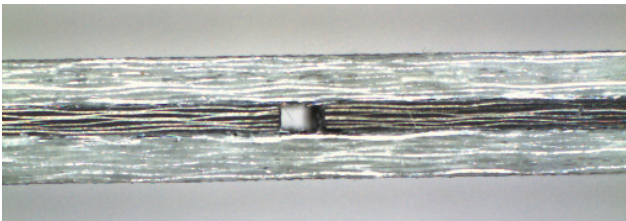

Figure 14: Picture of specimen 2 at 28578 N

The brighter appearance of the glass fibre adherend in Figure 14 is a result of inter fibre failure. Above a displacement of $u = 1.65$ mm a second linear slope is observable. This is due to the fact that at the end of the delamination process only the continuous layers are loaded. Due to the design of the specimen with the same extensional stiffness of each adherend, the extensional

stiffness is half the stiffness of the first linear slope. Using the load $N_x = 27500$ N and equation (26) and (27) the energy release rate G_c is 1.83 N/m and u_c is 0.87 mm. The displacement u_c is not explicit observable in Figure 12. The deformation of the testing machine is also measured. The stiffness change of the adherends followed by inter fibre failure is also a reason.

4 Comparison of numerical Analysis and Experiment

The analysis is made with $n = 100$ transfer units and 1000 displacement increments. The strength τ_{max} is assumed to be equal to the interlaminar shear strength of CFRP and set to 85 N/mm^2 [14]. The comparison of numerical analysis and experiment is shown in Figure 15.
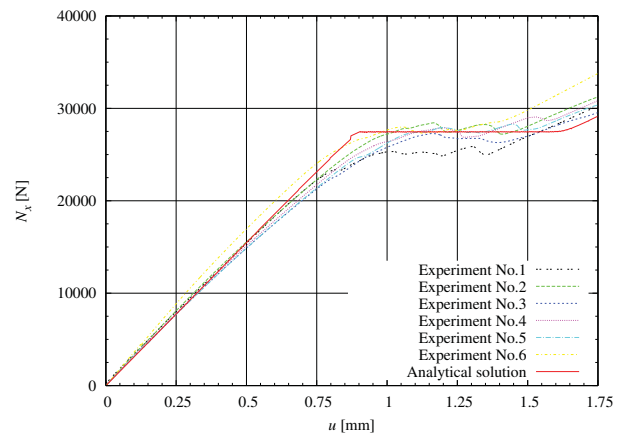

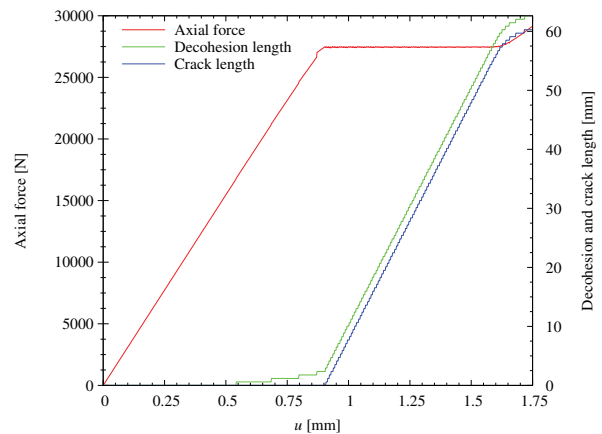Figure 15: Comparison of experiment and numerical analysis

Figure 16: Decohesion length and crack length

From $u = 0$ to $u = 0.8$ mm a linear increase of load with deformation is visible. The difference to the experimental results above a displacement of $u = 0.5$ mm is based on stiffness change caused by inter fibre failure of the glass fibre adherends.

This process is not considered by the used model of an elastic bar for the adherends. A constant load level at 27500 N and the beginning of the plateau at a

displacement of $u = 0.85$ mm is also observable, as well as a second linear area above $u = 1.65$ mm.

Figure 16 shows a computation of the decohesion length and the crack length. The decohesion process starts at a displacement of $u = 0.54$ mm. The fracture process starts at a displacement of $u = 0.90$ mm, which is close to $u_c = 0.87$ mm.

5 Conclusion and outlook

The presented paper shows the use of decohesion models to get an analytical solution to the analysis of delamination in composite structures. A bonded joint with two adherends and an adhesive layer is considered. The adherends are described by the theory of an elastic bar combined with a decohesion model to describe the shear stresses. The resulting system of differential equations is solved and leads to the transfer matrix method. The numerical results are compared with experimental results.

The use of an interface decohesion model combined with the theory of an elastic bar is a very efficient solution process to analyse delamination. The comparison of the numerical computed displacement and axial force shows a good agreement with the experimental results. The difference between numerical results and experiment can be explained by the neglect of inter fibre failure, which can be regarded in further models. A computation of the damage area and the fracture area is also possible, but the validation of this possibility has to be proven by experimental results.

For the joint, which is demonstrated in Figure 1, the neglect of normal stresses is not valid. Peeling stresses lead to an earlier collapse of a structure. The model has to be upgraded in order take normal stresses into account

6 References

[1] Alfano, G.; Finite Element Interface Models for the Delamination Anaylsis of Laminated Composites: Mechanical and Computational Issues; International Journal for numerical methods in engineering; 50; 1701-1736; 2001

[2] Bansemir, H.; Krafteinleitung in versteifte orthotrope Platten; Ingenieur-Archiv; 42; 127-140; 1973

[3] Bigwooda, D.A.; Elastic analysis and engineering design formulae for bonded joints; International journal of adhesion and adhesives; 9; 229-242; 1989

[4] Dávila, C.G.; Mixed-Mode Decohesion Elements for Analyses of Progressive Delamination; NASA Langley Research Center; 42nd AIAA/ASME/ASCE/AHS/ASC Structures; 2001

[5] Goland, M.; The stresses in cemented joints; Journal of applied mechanics; 11; A17-A27; 1944

[6] Gross, D.; Technische Mechanik 2; Springer-Verlag; Berlin, Deutschland; 1988

[7] Needleman, A.; Micromechanical modelling of interfacial decohesion; Ultramicroscopy; 40; 203-214; 1991

[8] Pestel, E.; Matrix-Method in Elastomechanics; McGraw-Hill; USA; 1963

[9] R&G; Faserverbundwerkstoffe Handbuch; R&G Faserverbundwerkstoffe GmbH; Waldenbuch, Deutschland; 2009

[10] R&G; Datenblatt Epoxidharz; R&G Faserverbundwerkstoffe GmbH; Waldenbuch, Deutschland; 2010

[11] Rapp, H.; Analysis of Delamination and bonded joints; Deutscher Luft- und Raumfahrtkongress; Aachen; 2009; ID 121190

[12] Tsai W.S.; Introduction to composite materials; Technomic Pulbishing Company; Westport, Connecticut, USA; 1980

[13] Williams, J.G.; On the calculation of energy release rate for cracked laminates; International Journal of Fracture; 36; 101-119; 1988

[14] Luftfahrttechnisches Handbuch; Band Faserverbund-Leichtbau; 1994